Polymer Bulletin (2022) 79:1929–1947
https://doi.org/10.1007/s00289-021-04013-0

ORIGINAL PAPER

# Modeling the mechanisms for formation of helices and perversions in elastic nanofilaments through molecular dynamics

**J. P. T. Lopes[1] · Fernao Vistulo de Abreu[2] · Ricardo Simoes[1,3]**

Received: 24 June 2021 / Revised: 23 November 2021 / Accepted: 3 December 2021 /
Published online: 10 January 2022
© The Author(s), under exclusive licence to Springer-Verlag GmbH Germany, part of Springer Nature 2021

## Abstract

Helices made of polymeric elastic filaments have been the target of considerable and growing interest in past years, given several potential applications. Although the underlying mechanisms responsible for the formation of such helices are still not sufficiently understood, recent results suggest they may result from buckling instabilities emerging from torsion in the extremities or when there is asymmetry across the filament's cross section. Also, the occurrence of perversions (regions where the helical handedness changes) has attracted considerable interest in a number of theoretical works, but the possibility of creating more than a single perversion, and thus control the geometry of helices and perversions in the resulting filament, has been given much less attention, despite its clear importance. In this paper, we present coarse-grained Molecular dynamics (MD) simulations that show it is possible to replicate the formation of helices and perversions within certain conditions, and which complement information available from experimental approaches. We show how the helical radius can depend on the strength and the asymmetry of the pairwise interactions, the filament's aspect ratio, and the strain rate of recovery, and we discuss in detail how perversions occur. The bonding potential parameters were found to have a small effect on the number of perversions, while the strain rate exhibited a significant effect, namely, an increase in 200-fold of the strain rate can induce as many as eight times more perversions for an aspect ratio of 200 (and three times more perversions for an aspect ratio of 50). The increase in the pair-wise interaction stiffness leads to lower loop diameters and higher number of loops, while an increase in the pair-wise equilibrium distance leads to larger loop diameters and consequently a lower number of loops; however, both these parameters exhibit a strong dependence on the aspect ratio. It was also found that an increase in the surface modification by 30% leads to an increase in circa 2.3 times the number of formed loops, while the average loop diameter decreases by circa 40%. From these results emerges a better understanding of how to tailor the geometry of the studied polymer elastic filaments, vital information for the design of next-generation nano-mechanical systems, such as those obtained by nano-patterning of soft materials.

Extended author information available on the last page of the article

**Graphical abstract**

Different number of perversions resulting from different strain rates during deformation (strain rate of case a is 200 times that of case b)

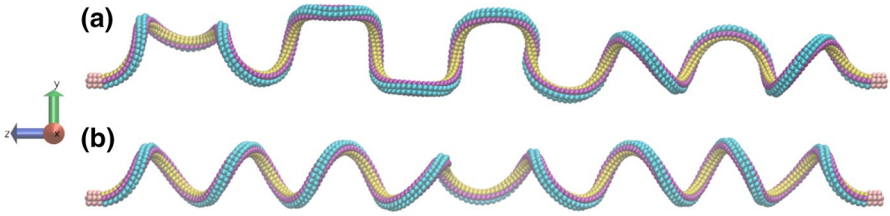


## Introduction

Since the discovery of helically coiled plant tendrils, there has been great interest in the study of the mechanisms that create these helicoidally shapes both from mechanical and functional perspectives, given the potential application of helices made of elastic filaments [1–3]. The most important of these works was made by Darwin in 1876 [4], when he observed that the tendrils of climbing plants often assume configurations consisting of subsequent helices of opposite handedness. The formation mechanisms for such helices are still not well understood, but recent results have indicated they may be due to buckling instabilities that naturally emerge when there is torsion in the extremities or asymmetry across the filament's cross section. Several different treatments (e.g., thermal, friction or radiation) can induce such asymmetry, which means this can be easily obtained in practice [5, 6]. In addition, these effects can be observed on filaments at different length scales; both micro-filaments and nano-filaments form this sort of structure.

The transition between the different helical segments is referred to as "perversion." Perversion is a classical pattern that can be observed in naturally curved rods. It consists of a junction between two helices with opposite chiralities. Similar configurations can often be observed for example in tangled phone cords or in electrospun fibers. Chirality is also frequently observed for cellulose-based helices in plants and has been shown to be reversible [7]. Perversions are shown to occur in the stationary solutions of Kirchoff's equations [8–10] and belong to a general class of solutions that can be derived in nonlinear analysis by connecting two competing equilibrium configurations, which are here the right-handed and left-handed helices in the presence of natural curvature. A study on cucumber tendrils [1] clearly shows that tendril coiling occurs via asymmetric contraction of an internal fiber ribbon of specialized cells. In the coiled shape, we can see different internal cells near one side of the surface, which indicates that through surface modifications, we can obtain helically coiled shapes from straight filaments. However, the possibility of creating more than a single perversion has been given much less attention [11]. Periodic tendril perversion has also been observed in crystalline chain structures, based

on various compounds, and again asymmetries are reported to play a role in the formation of the helical structures and perversions [12].

In the past decade, Reneker et al. described how micro-helical structures could be produced with different materials [13]. Later on, Yu et al. [14] reported on the fabrication of micro-helical structures with controlled helical pitches and using an ingredient familiar to the textile industry, polycaprolactone (PCL). In this work, optical images are shown with several entangled helices. Nevertheless, that work does not study how helices become entangled or what are the relevant mechanical properties of the resulting materials. In the literature, some other works reported the production of helical fibers by electrospinning [15, 16]. However, in those papers, the fabrication process is not clearly detailed, and the available control over the helical parameters does not seem as good. Thus, there is much room for improvement in terms of understanding the relevant parameters governing these processes. For those reasons, computer simulations will become more important in predicting the properties and behavior of these materials. A review on available electrospinning procedures which can be employed for creating helical shapes similar to those found in natural materials has been provided by one of us [17]. That review also describes in detail electrospinning methods reported in scientific literature for a variety of polymers which have been electrospun into fibers with diameters ranging from the nano- to micrometer size. A very recent review on electrospinning as a means to obtain functional materials shows potential applications and production methods [18], highlighting the importance of better understanding the underlying mechanisms.

Theoretical studies for the formation of helical shapes are based on early finite-element method of Kirchoff's rod model, but since the development of this model, several researchers have studied and enhanced it [8–10]. Domokos et al. [11] investigated mechanical spatial equilibrium of finite slender elastic rods with intrinsic curvature with clamped–clamped boundary conditions and found that one can obtain multiple perversions and that these appear in an arbitrary number and are connected by helical segments of arbitrary length. Nowadays, several studies accept and show that the anisotropy on the surface can create helically shaped materials. Studies made by Wang et al. [19, 20] using Kirchoff rod models suggest that one can design and adjust the morphology of synthesized nanohelices by tailoring or functionalizing their surfaces during fabrication. Huang et al. [21] also studied anisotropy using finite-element methods and surprisingly show that when joining a pre-strained elastomeric strip to another (unstrained), and then releasing the bi-strip, it results only in subsequent perversions, without the presence of helical segments. Also, they found that a helical loop has a lower energy than a perversion and that there is an energy barrier between a perversion and a helical loop.

Other relevant studies to mention are those on motion of flexible filaments [21–23], where symmetry breaking was shown to affect snaking-rotation transition. However, in those studies, it is hydrodynamic interaction that maintains rotation curvature of a filament. Also pertinent is the work of Isele-Holder et al. [24] on stable spiral formation of single flexible filaments, albeit using 2D Brownian dynamics simulations. Here, the dilute self-propelled filaments give rise to spontaneous formation and break-up of spirals. Also interesting is the prediction of curvature using beam theory with polymeric bilayers, namely for polyolefin thermoplastic

elastomers, where the authors found curling and twisting after high strain deformation and subsequent release [25]. Last, Wada [26] proposed an analytical model to predict the emerging helical structure in thin elastic composites, where the twisting and bending mechanisms were found to be influenced by the stiffness of the material and the induced strain.

In polymer science, entanglements have been described according to the reptation model [27]. Consequently, they are understood as fluid dynamical links, that can be destroyed and created in time and which can be best used to describe viscoelastic properties of materials. However, in a rapid communication to Soft Matter [28], it was shown that physical interactions alone can produce stable and localized links in helical structures, indicating the existence of another type of entanglement. These localized entanglements were called Physical PseudoKnots, PPKs. The new finding was experimentally validated with mechanical springs, where it was shown that the energy required to form PPKs could be at least two orders of magnitude smaller than the energies required to destroy them. PPKs can be widely observed in the macroscopic world in helical structures, like springs. PPKs use only physical interactions and are generated with little energy through a ratchet mechanism. This mechanism establishes that only for certain helical pitch to helical radius ratios can PPKs be formed. As a first step before attempting to explain the mechanisms behind the formation of PPKs, the present work is focused on the formation of helical structures from linear elastic filaments.

We intend to study this phenomenon through Molecular dynamics (MD), which was introduced by Alder and Wainwright in 1950, allowing the study of material behavior at the molecular level [29]. Nowadays, MD is widely used for simulations of material systems from the atomistic level to the mesoscale. One of its main advantages is that time is an explicit variable, allowing simulations of equilibrium properties and time-dependent ones; this is an essential characteristic for the simulation of viscoelastic materials, as shown in several polymer mechanical studies [30–40]. MD not only predicts the exact configuration of a system at a given time instant, but also allows estimating the system behavior through statistical or averaging methods [41]. Therefore, the macroscopic properties arise as averages along a statistical representative group of the molecular systems in equilibrium or non-equilibrium. However, MD simulations are limited to systems with relatively small timescales, particle numbers and steps without the loss of atomic resolution, even when acceleration techniques are used [42].

The main objective of this work is to develop molecular dynamics simulations that from linear filaments spontaneously create the aforementioned helically coiled shape filaments and study how the relevant parameters affect the resulting geometry. From this, the dynamics of perversions in electrospun fibers will become better understood. For the simulation, we change the bonding parameters on the surface of the filament and probe the resulting number of perversions, number of loops and helical diameters of different filaments.

In Sect. "Simulation model", we describe the simulation model employed, as well as the key parameters used in the simulations. In addition, we explain the simulation procedure and the simulation outputs. Subsequently, in Sect. "Results", we discuss the obtained results, focused on the effect of strain rate, extent of surface

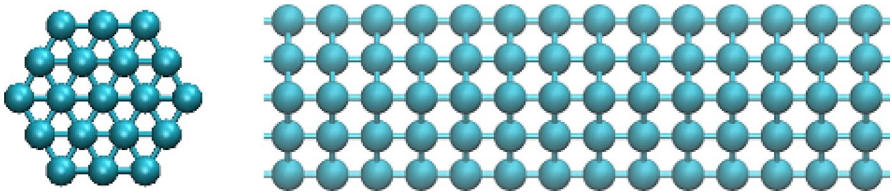

**Fig.1** Hexagonal model: transversal and longitudinal views, at the left and right, respectively

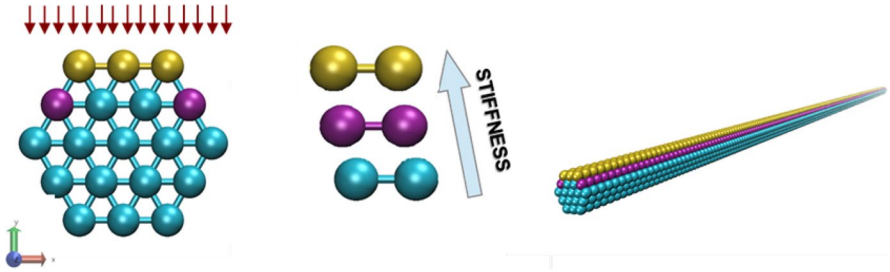


**Fig.2** Surface modification representation. Blue spheres represent the unmodified original segments, gold spheres represent the modified surface, and pink spheres represent the intermediate segments (partially affected by the surface modification, e.g., irradiation, and thus with intermediate stiffness)

modification, and bonding parameters. Finally, in Sect. "Conclusions", we present some concluding remarks and summarize the obtained results.

## Simulation model

### Model definition

We want to generate a rod-like fiber, and since we use a coarse-grained model, we developed a quasi-continuum rod, meaning that every particle is connected to its neighbors. Also, for purposes of simplification, we created a hexagonal rod, since this way, in the initial shape, all bonds are at the same distance and it becomes easier to model bonding asymmetries; see Fig. 1.

We then apply a surface modification along the fiber that experimentally could be achieved through radiation or chemical modification. This is obtained by changing the bonding potential in the surface, inducing anisotropy; see Fig. 2. As can be seen in Fig. 2, the surface modification is applied with two levels of intensity to create a softer transition.

In this study, we want to show that only through bonding and non-bonding potentials, without angular or dihedral potentials, we can induce a helical configuration in an elastic fiber. This would prove that the helical twisting arises only through bending asymmetries.

### Simulation parameters

While in previous publications [35], we employed our own molecular dynamics simulation code, in this work, we used LAMMPS [43] (Large-scale Atomic/Molecular Massively Parallel Simulator) to execute the molecular dynamics simulations. This will enable easier reproduction or continuation of this work by other authors. LAMMPS is a free open-source code and is designed to be easy to modify or extend with new capabilities, such as new force fields, atom types, boundary conditions, or diagnostics, making this program a very versatile tool.

To reproduce the simulation procedure in LAMMPS, it was needed to develop a script containing all the parameters and constraints described above. Also, we registered the beads trajectories for the purpose of visualization, calculating helical diameter, spring forces, lengths, volume, etc.

For the visualization of the simulation trajectories, we used VMD (Visual Molecular Dynamics) [44], an open-source program which allows visualizing the results of the simulation exported to a text file, and which is very well integrated with LAMMPS results files. We have also used the pizza.py Python scripts for pre- and post-processing of LAMMPS data (freely available at https://lammps.github.io/pizza/).

All values used throughout this article are in reduced units. For time integration, LAMMPS uses a standard velocity Verlet scheme (simulation time step of $1 \times 10^{-3}\ \tau$). The boundary conditions used in the simulations were non-periodic shrink-wrapped, meaning the simulation box expands or contracts with the motion of the particles.

The simulations were done in the canonical ensemble, i.e., with constant number of particles N, constant volume V, and constant bath temperature T. For this purpose, we used a Nosé–Hoover thermostat with temperature equal to 0.005 and with a damping value of 0.001 (a low temperature to have a sort of glassy state).

The Lennard–Jones force field potential was used to define the intermolecular or secondary interactions (bonds). This potential is also widely used to describe this type of interaction (non-bonding interactions) in MD simulations [45]. There are some variants of this potential, typically the most used and the one adopted in this study is the Lennard–Jones 12–6, described by:

$$E_{LJ12-6} = \begin{cases} 4\varepsilon[(\sigma/r)^{12} - (\sigma/r)^{6}], r < r_c \\ 0, r \geq r_c \end{cases} \tag{1}$$

Here, $r$ is the distance between a pair of non-bonded particles, and the parameters $\varepsilon$ and $\sigma$ are the energy well depth and the distance between particles at which the energy becomes zero, respectively. Typically for computational efficiency, this potential has a cutoff distance, meaning that from this distance, further, the potential is equal to zero, which is not calculated by the program. The coefficients chosen for this potential are their canonical values: $\sigma = 1$; $\varepsilon = 1$; $r_c = 1.8$. The employed cutoff distance results from years of experience of the authors with molecular dynamics simulations using Lennard–Jones potentials [35–37].

**Table 1** Parameters used in the simulations

| Diameter *(ϕ)* | Aspect ratio (L/D) | K1/K0 | Modified surface (%) | σ1/σ0 |
|---|---|---|---|---|
| 3 | 50; 100; 200 | 0.5; 1; 1.5; 2 | 57 | 0.66; 0.75; 0.83 |
| 5 | 50; 100; 200 | 0.5; 1; 1.5; 2 | 16; 26; 36; 47 | 0.75 |

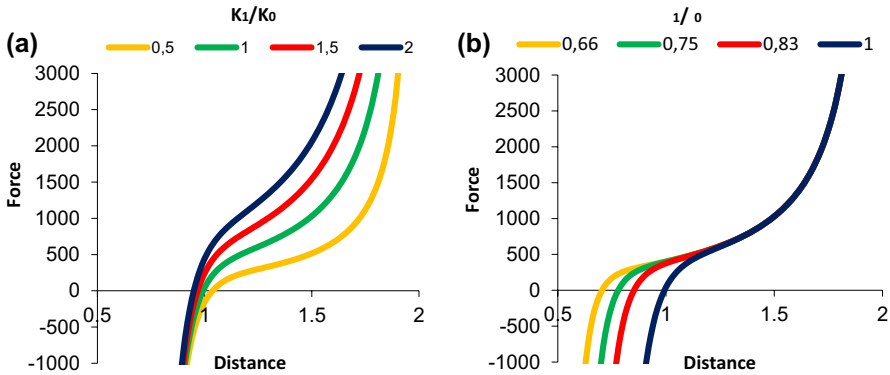


**Fig. 3** FENE bond potential with different K ratios (**a**) and σ ratios (**b**)

The force field potential chosen to define the intramolecular or primary interactions was the FENE (Finite Extensible Nonlinear Elastic) bond potential, developed by Kremer and Grest [46–48]. This potential is widely used in MD and is defined by the following equation:

$$E_{bond} = -\frac{1}{2}K_0{R_0}^2 ln\left[1-\left(\frac{r}{R_0}\right)^2\right] + 4\varepsilon[(\sigma/r_{LJ})^{12} - (\sigma/r_{LJ})^6] + \varepsilon, \mathrm{r} < R_0 \quad (2)$$

where $r$ is the distance between a pair of bonded particles. Here, $r < R_0$, where $K_0$ is a spring constant and $R_0$ is the maximum extent.

For the unmodified part of the filament, the coefficients used for the simulation are $K_0 = 150$; $\sigma = 1$; $\varepsilon = 1$; $R_0 = 1.2$. The average bond length with these parameters is$0.97\sigma$. The values used for the modified surface ($K_1$) are with respect to the unmodified part ($K_0$) and are described by their ratios as shown in Table 1. The values of the aspect ratio were selected based on ranges in natural materials such as wood cellulose nanofibers [49, 50], the extent of surface modification comes from experimental work done by some of us and collaborators [17, 51], and the K and σ values come also from previous work with MD by some of us and collaborators [35–37].

As seen in Table 1, the parameters studied are the fiber aspect ratio and K bonding parameter effect. The σ parameter effect was only studied for diameter 3. The extent of surface modification was studied only for diameter 5.

Looking at Fig. 3a, it can be easily seen that by changing K, the attractive part of the potential is changed; higher K makes it harder to stretch a bond from the

**Fig. 4** Perversion observed in the process of curling and wrinkling of an electrospun fiber (authors' image)

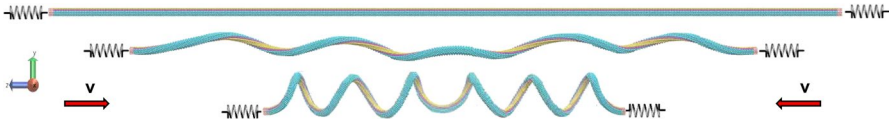


**Fig. 5** Simulation procedure. Blue spheres represent the unmodified original segments, gold spheres the modified surface, and pink spheres intermediate segments

equilibrium distance (where Force = 0). The σ ratio changes only the equilibrium distance, but keeping the shape of the curve, as shown in Fig. 3b.

## Simulation procedure

To gain insight on the helical formation behavior, we use an approach that allows the formation of helical perversions, such as those observed in both natural and artificial systems (see Fig. 4).

Perversions can be produced by first flattening a helical spring into a flat straight filament by pulling on both its ends (see Fig. 5–top) and progressively releasing its ends from this straight configuration with clamped–clamped boundaries (see Fig. 5–center), until a shape made of two mirror-symmetric helices is obtained (see Fig. 5–bottom). The velocity of the ends release is vital in the dynamical behavior of this procedure. The existence of perversions is due to the nonlinear behavior of the rod. This mechanism usually generates one perversion in the middle, but occasionally can produce more than one perversion.

Here, we use steered molecular dynamics [52], applying mechanical springs to hold both ends of the filament, and defining an end-release velocity which will be termed strain rate. Note how different this is from contorting a naturally curved elastic rod, such as in the work presented by Lazarus et al. [53], where rotation is imposed externally rather than generated solely from the fiber asymmetry. Note that, the material is initially allowed to recover to a minimum energy configuration (after the lattice-based fiber creation procedure), before the fiber ends are allowed to move.

The springs are applied to allow conformational changes in the filament and easily remove excess energy due to temperature and/or spring movement. The springs are defined by a restoring force of magnitude $F_{spring} = k\left(\mathrm{R} - R_0\right)M_i/\mathrm{M}$ which is applied to each atom in the group where $k$ is the spring constant, $M_i$ is the mass of the atom, and M is the total mass of all atoms in the group. Note that, $k$ thus represents the total force on the group of atoms, not a per-atom force. The equilibrium position of the spring is $R_0$. To define a specific strain rate, the spring equilibrium position is progressively changed along time.

As mentioned above, the strain rate is very important in defining the final helical shape; we will show that this parameter is fundamental to obtain one or more perversions.

In order to probe the helical formation mechanisms, we studied this approach with different filaments varying diameter and aspect ratio, different surface modifications varying primary interactions strength and the extent of the modified surface, and varying the strain rate. Note that, the described surface modification can be achieved through many different types of mechanisms and it is outside the scope of this paper to discuss such mechanisms or explore their influence of the resulting surface properties.

## Results

First, we show how more than one perversion can be obtained; mainly this is given by changing the strain rate and the aspect ratio. We then show the results concerning the number of helical loops and the helical diameter. For comparison, we chose the configurations that have only one perversion. This allows insight on the bonding values for producing different sized helices.

The extent of surface modification is studied and then we show that the bonding parameters ratios of the modified/unmodified structure give rise to different size/shape helicoidal filaments.

For studies focused on fibrous aggregates of multiple helically wound filaments, rather than perversions, the reader is referred to the work of Gruziel and Szymczak [54], who used the same molecular dynamics and visualization packages (LAMMPS and VMD), as well as a course-grain simulation model.

### Strain rate effect

First, we studied the velocity effect because in order to be able to study the diameter and number of loops with the defined procedure (independently), it is important to obtain only one perversion. It should be mentioned that in one or two cases, this could not be achieved, due to the fiber length, as explained in more detail below. The parameters maintained were the diameter of 3 statistical segments with the surface modification of 57% (see top-right illustration in Fig. 6) and $\sigma 1/\sigma 0 = 0{,}75$.

Results clearly show that increasing the strain rate results in more perversions; see Figs. 6, 7, 8. This can be related to the expected energy barrier between the formation of a perversion and a loop reported by Huang et al. [21] that states that with higher energy strains, the helical loop is preferentially obtained. Also, they suggest that the velocity (strain rate) can influence the number of perversions obtained and our results confirm this.

The effect of different velocities is illustrated in Fig. 9. Also, this shows that it is easier to form perversions from a linear filament; however, by using the clamped–clamped constraints and given enough tiThe results show that for higher aspect ratios (see Fig. 8), it is harder to obtain only one perversion. This is because

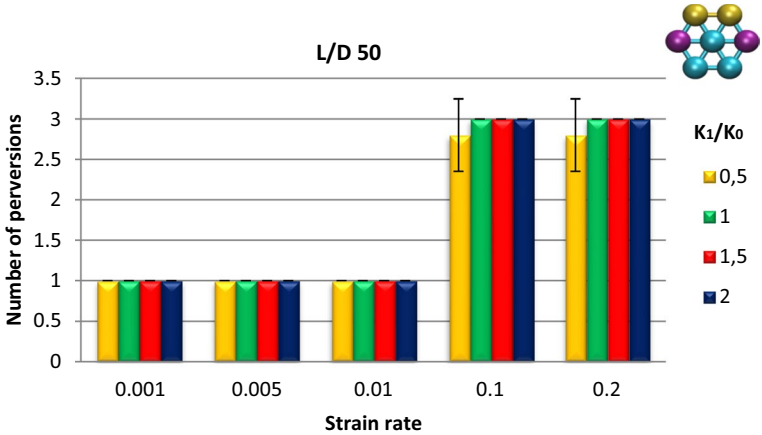


**Fig. 6** Perversions vs. Strain rate for different K ratios. In the cross-sectional view on the top right corner, the blue spheres represent the unmodified original segments, gold spheres represent the modified surface, and pink spheres represent intermediate segments

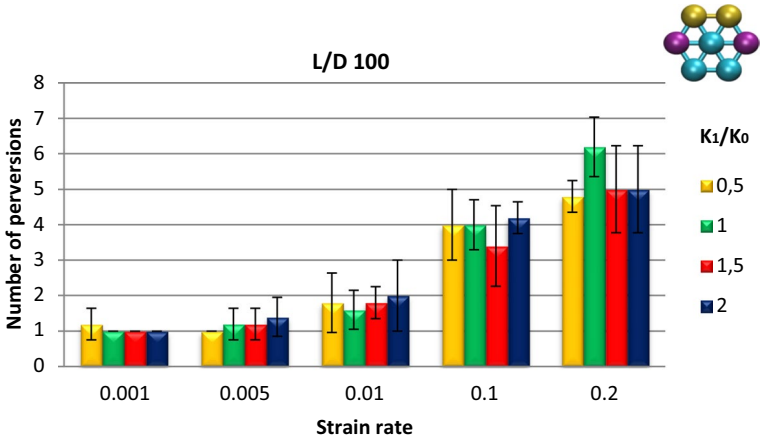


**Fig. 7** Perversions vs. Strain rate for different K ratios. In the cross-sectional view on the top right corner, the blue spheres represent the unmodified original segments, gold spheres represent the modified surface, and pink spheres represent intermediate segments

the energy associated with the perversions is lost along the filament length; thus, when the perversions are sufficiently far from another, they can be considered spatially uncorrelated. This shows that for higher aspect ratios, more perversions are obtained, even at small strain rates.

It should be mentioned that the two types of behavior described above can be seen in ribbons, such as those normally used for wrapping gifts.

me (lower strain rates), the perversions wind/unwind and become loops, which is a more stable local configuration.

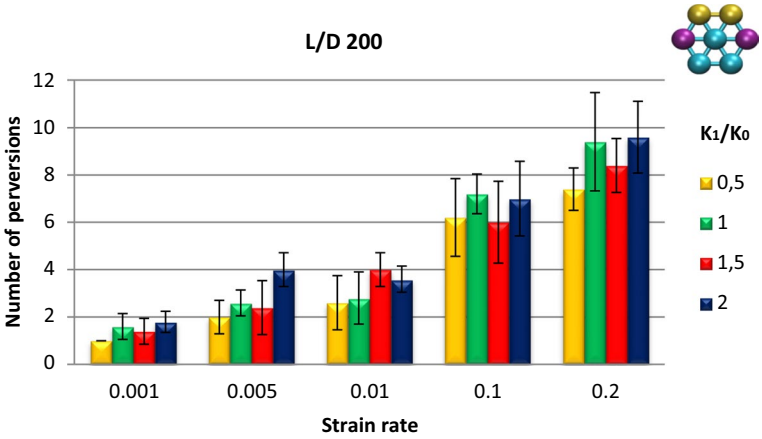


**Fig. 8** Perversions vs. Strain rate for different K ratios. In the cross-sectional view on the top right corner, the blue spheres represent the unmodified original segments, gold spheres represent the modified surface, and pink spheres represent intermediate segments

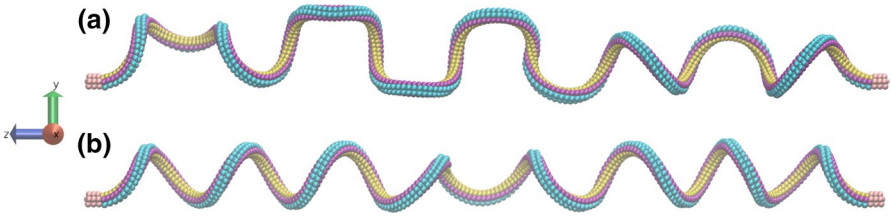


**Fig. 9** Different strain rates and the respective difference in number of perversions. **a** v = 0,2 and **b** v = 0,001. All simulation parameters are the same in **a** and **b**, namely D = 3; L/D = 100; K1/K0 = 1. Blue spheres represent the unmodified original segments, gold spheres represent the modified surface, and pink spheres represent intermediate segments

From these results, we chose a reasonable strain rate for subsequent studies, in order to obtain the fewer perversions possible, preferably only one perversion. Thus, in the simulations shown in the next sections, the strain rate is always 0.001.

## Surface modification extent effect

For this study, only fibers with diameter of 5 statistical segments were used, since these allow for different surface modification configurations (see Fig. 10). The bonding parameters are K1/K0 = 1 and σ1/σ0 = 0,75 and, as mentioned before, the intermediate (purple) beads have a σ1/σ0 of 0,83.

The simulations results show that a higher level of surface modification results in more loops and, consequently, lower helical diameters. Also, the trends are consistent for this study. The behavior is shown in Fig. 11. On average, an increase from 16 to 47% modified surface leads to an increase in about 2.5 times

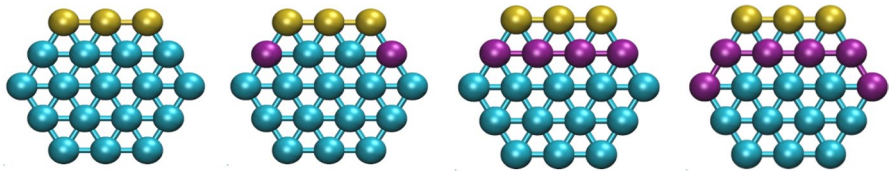

**Fig. 10** Different surface modifications: 16, 26, 36 and 47%, from left to right, respectively. Blue spheres represent the unmodified original segments, gold spheres represent the modified surface, and pink spheres represent the intermediate segments (partially affected by the surface modification, e.g., irradiation, and thus with intermediate stiffness)

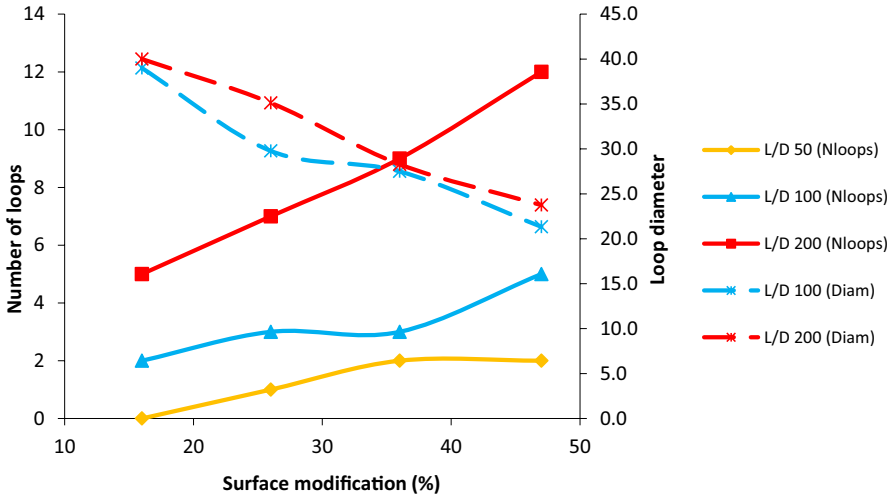


**Fig. 11** Extent of surface modification vs. number of loops and loop diameter, in solid line and dashed line, respectively

more loops (in the case of the smaller aspect ratio fiber, no loop is observed at the minimum extent of surface modification). Conversely, that increase in the modified surface from 16 to 47% leads to a decrease in the diameter of the loops of 56% (on average). These trends were also found to be near linear ($R^2 > 0.9$).

The explanation to this phenomenon is that by having more modified (stiffer) particles, the upper part of the filament has a larger tendency to shrink, and due to the non-modified particles competition, this will result in helices with more loops and lower diameters.

For the aspect ratio of 50, it was not possible to accurately measure the diameter for the lower surface modification since it has very few loops; in Fig. 12, it can be seen how the diameter changes.

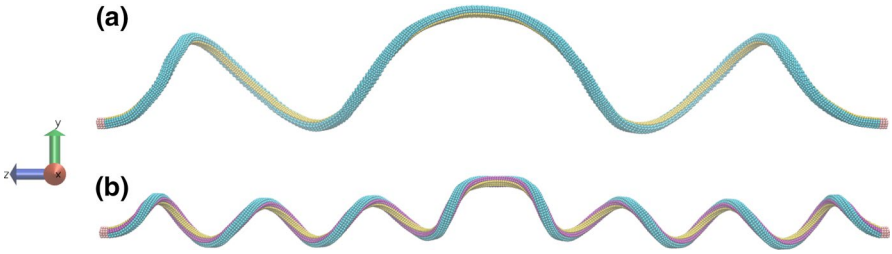


**Fig.12** Fiber configuration for different extents of surface modification: **a** 16% and **b** 47%. All simulation parameters are the same in **a** and **b**, namely D = 3; L/D = 100; K1/K0 = 1. Blue spheres represent the unmodified original segments, gold spheres represent the modified surface, and pink spheres represent intermediate segments

## σ ratio effect

For this study, we evaluate the σ ratio effect for filaments with diameter of 3 statistical segments, surface modification of 57% and K1/K0 = 1.

The results show that for higher σ ratio, we obtain larger diameters and fewer loops. This is explained by the tension that the stiffer part of the fiber (smaller σ) is under, thus leading to a larger contraction of this area and, as seen in Fig. 13, to higher diameters and fewer loops.

On average, an increase in σ1/σ0 from 0.66 to 0.83 increases the diameter of the loops by approximately 54%. Conversely, the number of loops is reduced by approximately 40% (consistently for the different aspect ratios). Naturally, many more

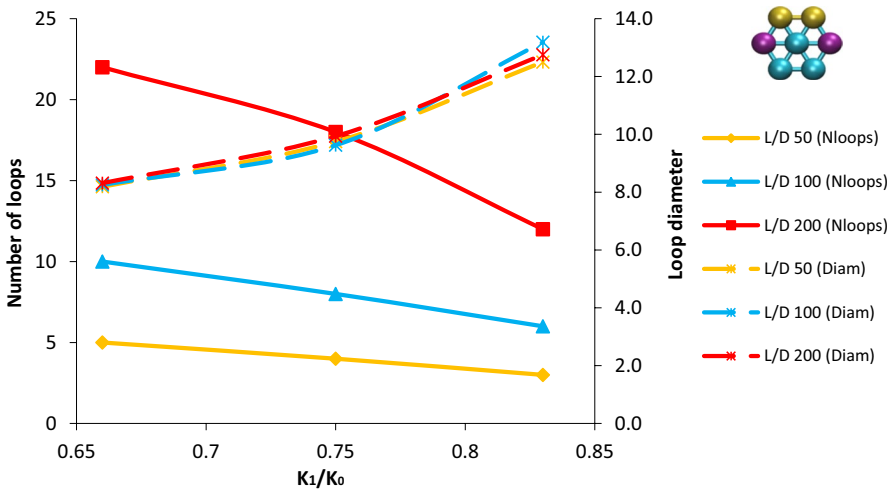


**Fig. 13** Bonding parameter σ vs. number of loops and loop diameter, in solid line and dashed line, respectively. In the cross-sectional view on the top right corner, the blue spheres represent the unmodified original segments, gold spheres represent the modified surface, and pink spheres represent intermediate segments

loops are observed for higher aspect ratio fibers (the number of loops increasing almost linearly with the aspect ratio). In terms of the molecular dynamics simulation, the σ1/σ0 ratio increase corresponds to longer bond equilibrium distances, thus allowing larger loops to form.

These results also reveal that the aspect ratio has no influence in the helical diameter obtained. The slight differences in diameter are due to the initial small random perturbation from ideal lattice positions of the initial configuration, and essentially overlap for a large number of simulations with the same parameters.

## K ratio effect

To study the bonding parameter K effect on the final helical configuration, the chosen parameters were σ1/σ0 = 0,83 and surface modification of 57% and 26% for diameters of 3 and 5 statistical segments, respectively. Similarly to what was described in Sect. 3.2, the helical diameter for the lowest aspect ratio with filament diameter 5 is not measured.

The results, illustrated in Figs. 14, 15, show that as the ratio between the modified and unmodified bonds becomes larger (higher K1/K0), this results in smaller loop diameters and consequently more loops. On average, an increase in four times of K1/K0 (from 0.5 to 2) leads to an increase in two to three times of the number of loops. This effect is less pronounced as the fiber aspect ratio increases, and more pronounced as the diameter of the fiber increases. Conversely, with the increase in four times of K1/K0 (from 0.5 to 2), the diameter of the loops decreases by 35–40%. This effect is consistent for different aspect ratios and is less pronounced as the diameter

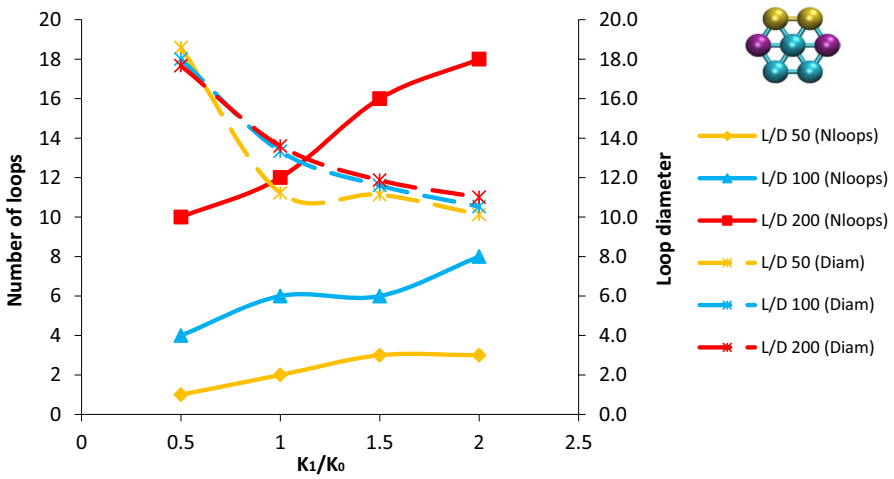


**Fig. 14** Bonding parameter K vs. number of loops and loop diameter, in solid line and dashed line, respectively. In the cross-sectional view on the top right corner, the blue spheres represent the unmodified original segments, gold spheres represent the modified surface, and pink spheres represent intermediate segments

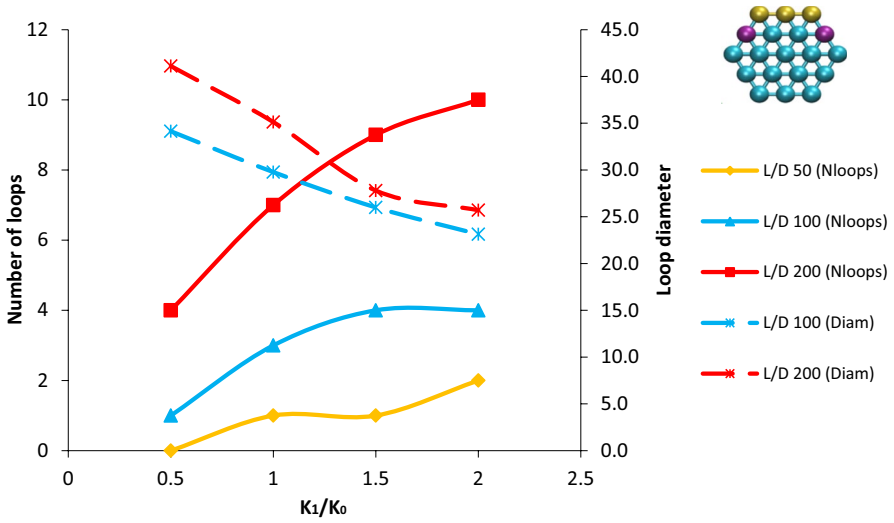


**Fig. 15** Bonding parameter K vs. number of loops and loop diameter, in solid line and dashed line, respectively. In the cross-sectional view on the top right corner, the blue spheres represent the unmodified original segments, gold spheres represent the modified surface, and pink spheres represent intermediate segments

of the fiber increases. In terms of the molecular dynamics simulation, the K1/K0 ratio increase corresponds to a stiffer bond (more difficult to stretch the bond beyond its equilibrium distance), which thus tightens the loops, reducing their diameter.

It is interesting to see that with the same equilibrium distance, and by changing only the stiffness of the bonds, we dictate the helical final configuration. Looking at the bonding potential (Fig. 4), we can conclude that the concurrence between the stiff and softer bonds becomes more pronounced if the strength of the bonds is different, i.e., if the softer surface has less bond strength, it cannot reach its equilibrium length while the stiffer part with higher bond strength contracts and compresses the filament further, thus leading to more loops and consequently lower diameters.

## Conclusions

The molecular dynamics method has been successfully employed to study the spontaneous formation of helices in elastic filaments. The proposed MD model can be compared visually and qualitatively to macroscopic situations. The simulations results reproduce the shapes observed experimentally, due to buckling instabilities that naturally emerge in elastic filaments when primary bond stiffness varies asymmetrically across the cross section, meaning that the helical twisting can arise only through bending asymmetries. This asymmetry can be obtained through thermal, friction or radiation surface treatments.

Moreover, we show that it is possible, by controlling the strain rate at which we allow the fiber to relax from extension, to obtain only one perversion for the

majority of fiber geometries. This study shows that to some extent, the number of perversions can be controlled, and that the strain rate is a critical parameter in controlling that number. This reinforces what has been reported by authors using simulations, although with harmonic interactions [55], on the role of strain rate in this type of microfilaments. It also expands on our earlier reports concerning the role of aspect ratio and extent of modified surface in the dynamics of formation of helix perversions [51].

We show that the number and diameter of helices depend on the material properties and fiber geometry. The concurrency between the stiffer and softer particles is determinant on the final helical diameter. The relation of this phenomenon and the initial aspect ratio dictates the final number of helices/perversions.

The strain rate exhibited a significant effect on the number of perversions, namely an increase in 200-fold of the strain rate can induce as many as eight times more perversions for an aspect ratio of 200 (three times more perversions for an aspect ratio of 50). The increase in the pair-wise interaction stiffness leads to smaller loop diameters and higher number of loops, while an increase in the pair-wise equilibrium distance leads to larger loop diameters and consequently a lower number of loops; however, both these parameters exhibit a strong dependence on the aspect ratio. It was found that an increase in the surface modification from 17 to 47% leads to an increase in circa 2.3 times the number of formed loops, while the average loop diameter decreases by circa 40%.

An increase in the bonding parameter ratio $\sigma 1/\sigma 0$ from 0.66 to 0.83 reduces the number of loops by approximately 40%, while their diameter increases by approximately 54%. An increase in the bonding parameter K1/K0 from 0.5 to 2 leads to an increase in 2–3 times of the number of loops, but their diameter decreases by 35–40%. The diameter of the loops is near independent of the fiber aspect ratio, while the number of observed loops naturally increases for higher aspect ratios.

These results contribute to a better understanding of the underlying mechanisms in the formation of helices and perversions in polymeric elastic filaments, paving the way to the design of the next-generation nano-mechanical systems obtained through nano-patterning of soft materials.

**Acknowledgements** This work is funded by FEDER funds through the COMPETE 2020 program and National Funds through the Portuguese Foundation for Science and Technology (FCT) to IPC under projects UIDB/05256/2020 and UIDP/05256/2020.

**Data availability** Data can be made available on reasonable request.

**Code availability** Simulations were performed using open-source software (LAMMPS).

## Declarations

**Conflicts of interest** The authors have no conflicts of interest to declare that are relevant to the content of this article.

## References


1. Gerbode SJ, Puzey JR, McCormick AG, Mahadevan L (2012) How the cucumber tendril coils and overwinds. Science 337:1087
2. Shariatpanahi SP, Iraji zad A, Abdollahzadeh I, Shirsavar R, Bonn D, Ejtehadi R, (2011) Micro helical polymeric structures produced by variable voltage direct electrospinning. Soft Matter 7:10548
3. Godinho MH, Canejo JP, Feio G, Terentjev EM (2010) Self-winding of helices in plant tendrils and cellulose liquid crystal fibers. Soft Matter 6:5965
4. Darwin C (1876) The movements and habits of climbing plants. Appleton, New York, 2nd ed.
5. Godinho MH, Trindade AC, Figueirinhas JL, Melo LV, Brogueira P, Deus AM, Teixeira PIC (2006) Tuneable micro- and nano-periodic structures in a free-standing flexible urethane/urea elastomer film. Eur Phys J E 21:319
6. Wilson DK, Kollu T (1991) The production of textured yarns by the false-twist technique. Text Prog 21:1
7. Almeida APC, Querciagrossa L, Silva PES, Gonçalves F, Canejo JP, Almeida PL, Godinho MH, Zannoni C (2019) Reversible water driven chirality inversion in cellulose-based helices isolated from Erodium awns. Soft Matter 15:2838
8. McMillen T, Goriely A (2002) Tendril perversion in intrinsically curved rods. J Nonlinear Sci 12:241
9. Nizette M, Goriely A (1999) Towards a classification of Euler-Kirchhoff filaments. J Math Phys 40:2830
10. Goriely A, Tabor M (2000) The Nonlinear Dynamics of Filaments. Nonlinear Dyn 21:101
11. Domokos G, Healey TJ (2005) Multiple helical perversions of finite intrinsically curved rods. Int J Bifurc Chaos 15:871
12. Hancock JC, Nisbet ML, Zhang W, Halasyamani PS, Poeppelmeier KR (2020) Periodic Tendril Perversion and Helices in the AMoO2F3 (A = K, Rb, NH4, Tl) Family. J Am Chem Soc 142:6375–6380
13. Han T, Reneker DH, Yarin AL (2007) Buckling of jets in electrospinning. Polymer 48:6064
14. Yu J, Qiu Y, Zha X, Yu M, Yu J, Rafique J, Yin J (2008) Production of aligned helical polymer nanofibers by electrospinning. Eur Polym J 44:2838
15. Xin Y, Huang ZH, Yan EY, Zhang W, Zhao Q (2006) Controlling poly(*p*-phenylene vinylene)/poly(vinyl pyrrolidone) composite nanofibers in different morphologies by electrospinning. Appl Phys Lett 89:053101
16. Shin MK, Kim SI, Kim SJ (2006) Reinforcement of polymeric nanofibers by ferritin nanoparticles. Appl Phys Lett 88:193901
17. Silva PES, de Abreu FV, Godinho MH (2017) Shaping helical electrospun filaments: a review. Soft Matter 13:6678
18. Xiuling Y, Jingwen W, Hongtao G, Li L, Wenhui X, Gaigai D (2020) Structural design toward functional materials by electrospinning A review. E-Polymers 20:682–712
19. Wang JS, Feng XQ, Wang GF, Yu SW (2008) Twisting of nanowires induced by anisotropic surface stresses. Appl Phys Lett 92:191901
20. Wang JS, Ye HM, Qin QH, Xu J, Feng XQ (2012) On the spherically symmetric Einstein–Yang–Mills–Higgs Equations in Bondi coordinates. Proc R Soc A Math Phys Eng Sci 468:609
21. Huang J, Liu J, Kroll B, Bertoldi K, Clarke DR (2012) Spontaneous and deterministic three-dimensional curling of pre-strained elastomeric bi-strips. Soft Matter 8:6291
22. Jiang H, Hou Z (2014) Motion transition of active filaments: rotation without hydrodynamic interactions. Soft Matter 10:1012
23. Jiang H, Hou Z (2014) Hydrodynamic interaction induced spontaneous rotation of coupled active filaments. Soft Matter 10:9248
24. Isele-Holder RE, Elgeti J, Gompper G (2015) Self-propelled worm-like filaments: spontaneous spiral formation, structure, and dynamics. Soft Matter 11:7181
25. Wisinger CE, Maynarda LA, Barone JR (2019) Bending, curling, and twisting in polymeric bilayers. Soft Matter 15:4541
26. Wada H (2016) Structural mechanics and helical geometry of thin elastic composites. Soft Matter 12:7386–7397
27. de Gennes PG (1971) Reptation of a Polymer Chain in the Presence of Fixed Obstacles. J Chem Phys 55:572
28. Abreu FV, Dias RG, von Ferber C (2008) Pseudo-knots in helical structures. Soft Matter 4:731
29. Gates TS, Hinkley JA (2003) Computational materials : modeling and simulation of nanostructured materials and systems. National Aeronautics and Space Administration, Langley Research Center, Hampton, VA.

30. Hossain D, Tschopp MA, Ward DK, Bouvard JL, Wang P, Horstemeyer MF (2010) Molecular dynamics simulations of deformation mechanisms of amorphous polyethylene. Polymer 51:6071
31. Tschopp MA, Bouvard JL, Ward DK, Horstemeyer MF (2011) Supplemental Proceedings, Vol 2: Materials Fabrication, Properties, Characterization and Modeling. John Wiley & Sons, 789–794.
32. Ge T, Robbins MO (2010) Anisotropic plasticity and chain orientation in polymer glasses. J Polym Sci Part B Polym Phys 48:1473
33. Hoy RS (2011) Why is understanding glassy polymer mechanics so difficult. J Polym Sci Part B Polym Phys 49:979
34. Hoy RS, Robbins MO (2006) Strain hardening of polymer glasses: Effect of entanglement density, temperature, and rate. J Polym Sci Part B Polym Phys 44:3487
35. Simoes R, Cunha AM, Brostow W (2006) Molecular Dynamics Simulations 0f Polymer Viscoelasticity: Effect of the Loading Conditions and Creep Behavior. Model Simul Mater Sci Eng 14:157
36. Simoes R, Cunha AM, Brostow W (2006) Computer Simulations of True Stress Development and Viscoelastic Behavior in Amorphous Polymeric Materials. Comput Mater Sci 36:319
37. Brostow W, Khoja S, Simoes R (2017) Sliding wear behavior of polymers studied with mesoscopic molecular dynamics. J Mater Sci 52:1203
38. Capaldi FM, Boyce MC, Rutledge GC (2002) Enhanced Mobility Accompanies the Active Deformation of a Glassy Amorphous Polymer. Phys Rev Lett 89:175505
39. Capaldi FM, Boyce MC, Rutledge GC (2004) Molecular response of a glassy polymer to active deformation. Polymer 45:1391
40. Hoy RS, O'Hern CS (2010) Viscoplasticity and large-scale chain relaxation in glassy-polymeric strain hardening. Phys Rev E 82:041803
41. Rudd RE, Broughton JQ (2000) Concurrent Coupling of Length Scales in Solid State Systems. Phys Status Solidi 217:251
42. Frederix K (2010) Structured Matrices and Their Applications. PhD thesis, Faculty of Engineering Science, KU Leuven.
43. Plimpton S (1995) Fast Parallel Algorithms for Short-Range Molecular Dynamics. J Comput Phys 117:1
44. Humphrey W, Dalke A, Schulten K (1996) VMD: Visual molecular dynamics. J Mol Graph 14:33
45. Peter C, Kremer K (2009) Soft Matter, Fundamentals and Coarse Graining Strategies. In: Multiscale Simulation Methods in Molecular Sciences, eds Grotendorst, J, Attig, N, Blügel, S Marx, and D, Forschungszentrum Jülich, vol 42, pp 337.
46. Grest GS, Kremer K (1986) Molecular dynamics simulation for polymers in the presence of a heat bath. Phys Rev A 33:3628
47. Kremer K, Grest GS (1990) Dynamics of entangled linear polymer melts: A molecular-dynamics simulation. J Chem Phys 92:5057
48. Auhl R, Everaers R, Grest GS, Kremer K, Plimpton SJ (2003) Equilibration of long chain polymer melts in computer simulations. J Chem Phys 119:12718
49. Iwamoto S, Lee SH, Endo T (2014) Relationship between aspect ratio and suspension viscosity of wood cellulose nanofibers. Polym J 46:73
50. Amiralian N, Annamalai PK, Garvey CJ, Jiang W, Memmott P, Martin DJ (2017) High aspect ratio nanocellulose from an extremophile spinifex grass by controlled acid hydrolysis. Cellulose 24:3753
51. Silva P, Trigueiros J, Trindade A, Simoes R, Dias RG, Godinho MH, de Abreu FV (2016) Perversions with a twist Sci Rep 6:23413
52. Izrailev S, Stepaniants S, Isralewitz B, Kosztin D, Lu H, Molnar F, Wriggers W, Schulten K (1999) Steered Molecular Dynamics. In: Computational Molecular Dynamics: Challenges, Methods, Ideas SE - 2, eds Deuflhard P, Hermans J, Leimkuhler B, Mark A, Reich S, Skeel R, Springer, Berlin Heidelberg, vol 4, pp 39.
53. Lazarus A, Miller JT, Metlitza MM, Reis PM (2013) Contorting a heavy and naturally curved elastic rod. Soft Matter 9:8274
54. Gruziel M, Szymczak P (2015) From ribbons to tubules: a computational study of the polymorphism in aggregation of helical filaments. Soft Matter 11:6294
55. Silva P, Godinho MH (2017) Helical Microfilaments with Alternating Imprinted Intrinsic Curvatures. Macromol Rapid Commun 38:1600700

**Publisher's Note** Springer Nature remains neutral with regard to jurisdictional claims in published maps and institutional affiliations.

## Authors and Affiliations

**J. P. T. Lopes[1] · Fernao Vistulo de Abreu[2] · Ricardo Simoes[1,3]**

✉ Ricardo Simoes
rsimoes@dep.uminho.pt; rsimoes@ipca.pt

[1] Institute for Polymers and Composites - IPC, University of Minho, Campus de Azurém, 4800-058 Guimarães, Portugal

[2] Departmento de Física/I3N, Universidade de Aveiro, Campus Universitário de Santiago, 3810-193 Aveiro, Portugal

[3] Polytechnic Institute of Cávado and Ave (IPCA), Campus do IPCA, 4750-810 Barcelos, Portugal